Mechanics of Advanced Composite Structures

Journal homepage: https://macs.semnan.ac.ir/

Semnan University

ISSN: 2423-7043

Research Article

Impact and Blast Resistance Enhancement of Reinforced Concrete Slabs Strengthened with CFRP and GFRP Systems: Experimental and Numerical Investigation

Hayder Abdul Hadi Abdul Razzaq *,

PhD in Structural Engineering, Lecturer, Islamic University of Al-Najaf, College of Engineering Technology, Department of Building and Construction Technology

ARTICLE INFO

Article history:

Received: 2025-11-7
Revised: 2026-1-28
Accepted: In Press

Keywords:

Dynamic Response
Composite Laminates
Energy Dissipation
Structural Resilience
Nonlinear Finite Element Modeling

ABSTRACT

Reinforced concrete (RC) slabs are widely used in critical infrastructure, yet they are vulnerable to sudden high-strain-rate loads such as low-velocity impact and blast. These hazards can induce brittle punching, large residual deformation, and loss of load-carrying capacity. This study evaluates the effectiveness of externally bonded fiber-reinforced polymers (FRP) for strengthening RC slabs against such actions. Nine slabs (1800 × 600 × 100 mm) were tested: three controls (unstrengthened), three strengthened with GFRP, and three strengthened with CFRP. Drop-weight impact tests were performed at energy levels ranging from 540 to 810 J. Results showed that CFRP strengthening reduced peak displacement by up to 28–35% and increased absorbed energy capacity by approximately 20–26% compared with control slabs. GFRP strengthening provided a smaller improvement, reducing displacement by only 10–14%. In addition, peak force resistance increased from an average of 48 kN (control) to 52 kN for CFRP-strengthened slabs. A calibrated nonlinear numerical model was developed to simulate both impact and idealized blast loading. The model predicted peak force and displacement values within ±8% of experimental results and confirmed the superior performance of CFRP layouts. The findings demonstrate that externally bonded CFRP is an effective retrofitting strategy for increasing the impact and blast resistance of RC slabs and improving structural resilience.

1. Introduction

Reinforced concrete (RC) slabs are fundamental components of critical infrastructure, including buildings, bridges, and protective facilities. Although these structural elements exhibit satisfactory performance under conventional loading, they are highly vulnerable to extreme dynamic actions, including impact and blast loads arising from vehicle collisions, accidental explosions, falling debris, or industrial incidents (Xie et al., 2025; Yazici & Özkal, 2025). Due to their relatively large exposed surface area. Under impact (sudden force) and blast (explosion-induced overpressure) loading,

* **Corresponding author.**
E-mail address: *alsedek.o.latof42992@st.tu.edu.iq*

conventional RC slabs often exhibit brittle behavior, failing suddenly with little deformation. This failure is characterized by shear failure (cracking due to sliding forces), concrete spalling (ejection of the surface layer), and severe fragmentation (breaking into pieces). These failure modes result in rapid loss of load-carrying capacity and the generation of high-velocity debris, posing serious risks to structural integrity and human safety. The limited ductility (ability to deform without breaking) and energy dissipation (absorption of dynamic forces) capacity of traditional reinforcement systems under rapid loading conditions highlight a critical weakness in existing infrastructure.

Externally bonded fiber-reinforced polymer (FRP) composite materials composed of strong, lightweight fibers embedded in a polymer matrix and attached to concrete surfaces have emerged as an effective strengthening solution due to their high strength-to-weight ratio, corrosion resistance (resistance to material degradation), and ease of installation. Numerous studies have demonstrated the benefits of FRP systems in enhancing the static (constant load), fatigue (repeated loading), and seismic (earthquake-related) performance of RC elements. However, the behavior of FRP-strengthened RC slabs under impact and blast loading remains insufficiently understood, as such extreme events involve fundamentally different failure mechanisms and strain-rate-dependent (sensitive to speed of load application) material responses.

Most existing investigations either focus on experimental impact testing or numerical blast analysis, with limited efforts to integrate both approaches. (Hosseini et al., 2023) There remains a significant challenge in developing validated nonlinear finite element models that can accurately simulate the interactions between concrete, steel reinforcement, FRP laminates, and adhesive interfaces under extreme dynamic loading. (Finite Element Modeling of Bond Behavior of FRP and Steel Plates, 2024) Particularly, there are a few instances where open-source computational frameworks transparently implement advanced constitutive laws and cohesive interface models. The key research gap is the lack of a comprehensive assessment of how FRP strengthening alters the failure mode from brittle to ductile under impact loading. (Nguyen et al., 2023)

The primary objective of this study is to conduct an integrated experimental (physical testing) and numerical (computer simulation) investigation into the effectiveness of externally bonded CFRP (carbon fiber-reinforced polymer) and GFRP (glass fiber-reinforced polymer) systems in enhancing the impact and blast resistance of RC slabs. The specific contributions of this work are to:

1. analyze the transition in failure modes induced by FRP strengthening, and
2. Develop and validate a Python-based nonlinear finite element (numerical analysis) framework incorporating strain-rate-dependent (loading-speed-sensitive) material models and cohesive interface behavior (bonding interaction), subsequently extending the validated model to predict blast response.

RC slab specimens strengthened with CFRP and GFRP sheets are experimentally tested using a controlled drop-weight impact setup. The validated numerical model is then employed to simulate blast loading using idealized pressure–time histories derived from established empirical formulations. The outcomes of this study provide an improved understanding of composite strengthening mechanisms and contribute to the development of resilient RC slab systems under extreme dynamic loading. The symbols and abbreviations used throughout the manuscript are summarized in the **List of Nomenclature,**
Novelty and Contributions of the Present Study

The novelty of this study lies in the combined experimental-numerical (physical tests and computer simulations) investigation of FRP-strengthened reinforced concrete slabs subjected to impact and blast loading, with explicit consideration of strain-rate-dependent (responsive to loading rate) material and interface behavior (bonding between materials). Unlike Zhong et al. (2023), who primarily employed idealized numerical simulations, our study provides experimentally validated insights into the mechanisms of failure mode transition and energy dissipation (loss of energy due to internal changes) under realistic dynamic loading conditions.

The main contributions of this study are summarized as follows:

1. Experimental quantification (measurement through testing) of impact response (reaction to sudden force) and energy absorption (ability to take in energy without failing) of CFRP- and GFRP-strengthened RC slabs under controlled drop-weight impact loading (precisely delivered dynamic loads).
2. Direct experimental and numerical (computer-simulated) evidence of failure mode transition from brittle (sudden and fragile) shear-dominated response to more ductile (deformable and flexible) behavior due to FRP strengthening.

3. Development and validation of a Python-based nonlinear finite element framework (computer code for simulating complex structural behavior) incorporating strain-rate-dependent (load speed-sensitive) constitutive models (material behavior equations) and cohesive interface behavior (bonding interaction).
4. Application of the validated numerical model (computer-based simulation) to assess blast response (structural reaction to rapid explosion pressure) within a defined range of charge weights (explosive amounts) and stand-off distances (distance from explosion to target).
5. Quantitative comparison (measurement-based evaluation) with previous studies, highlighting the influence of bond behavior (interaction at material interfaces) and strain-rate effects (loading-speed influences) on strengthening effectiveness.

2. Literature Review

The dynamic response of reinforced concrete (RC) slabs to impact and blast loading, with the severe structural damage and catastrophic consequences involved in such extreme events, has attracted much investigation. Both experiments and numerical studies proved that loads induce local failure modes-such as spalling or scabbing- that may later propagate into a total collapse situation. Wang et al. (2024) provided an explicit account of spalling-and-scabbing behavior in RC slabs under explosive loading, highlighting how these highly localized damages evolve into overall collapse. Low-velocity impact test results conducted by Anas et al. (2023) showed that an unstrengthened RC slab fails due to a shear-plugging mechanism at velocities higher than 5 m/s; thus, classifying the type/extent (severity) of fragmentation, which increases significantly with increasing impact energy. (2023) also found that a brittle shear failure dominates when the impact duration is shorter than the fundamental period of the slab. Ning et al. (2022) support this finding, reporting unprotected slabs with hazardous fragment velocities exceeding 200 m/s.

Many factors affect the dynamic response of RC slabs, including material strain-rate sensitivity and boundary conditions. At very high strain rates above 100 s^{-1}, concrete compressive strength has been reported to increase by up to 80%, while reinforcement yield stress increases by about 30% (Liu et al., 2022). Boundary conditions can be just as important, or even more so; Pham et al. (2021) found that clamped slabs have about 40% greater impact resistance than simply supported ones because membrane action develops in them.

FRP systems have been widely recommended as retrofit solutions to address the inadequate seismic vulnerability of RC slabs under extreme loading. Therefore, the behavior of stress transfer mainly through an adhesive bond at the interface between FRP and concrete governs that system. This has recently been quantified by De Maio et al. (2022) using a fracture mechanics approach under static loading conditions.[19] Dawood (2025) reported CFRP flexural strengthening could increase slab capacity up to 200% while Ombres et al. (2022) showed GFRP confinement resulted in high ductility enhancement; all three experiments were carried out on seismic load testing where Ortiz et al.(2023) [22] confirmed effectiveness results found previously by different researchers regarding inhibiting propagation shear cracks developing during cyclic loads applied Far less clear is the effectiveness of FRP strengthening under dynamic loading. Reifarth et al. (2021) found that CFRP strengthening can provide high blast resistance in close-in detonations, with premature debonding at pressures above 1 MPa. Said and Mouwainea (2021) show that FRP sheets offer very little resistance to low-velocity impact if delamination occurs early during loading. Numerical results by Almustafa and Nehdi (2021) indicate reductions as high as 60% in CFRP-strengthened displacements, assuming perfect bond conditions, which, according to them, is hardly ever realized experimentally; hence, their significantly different results bring out clearly the need for a more systematic investigation on bond integrity together with failure mode transition in FRP-strengthened slabs subjected to both impact as well as blast loading.

The phenomena described involve the development of advanced constitutive and numerical frameworks. A Concrete Damaged Plasticity (CDP) model is widely adopted to simulate concrete behavior under dynamic loading, including strain-rate effects as elucidated in Senthil et al. (2021). At ultra-high strain rates, the Johnson-Holmquist (JH2) model has been shown to better capture concrete fragmentation. Reinforcing steel is generally represented by a Cowper-Symonds formulation to capture dynamic hardening effects (Liu et al., 2022).In FRP-strengthened systems, the representation of the FRP-concrete interface is highly significant; cohesive zone models with rate dependency have been proposed recently for simulating debonding behavior (Shi et al., 2024); however, such models are often calibrated extensively within commercial finite element packages, and they have apparently inspired the emergence of open-source numerical frameworks as well. A Python-based finite

element platform with capabilities for simulating impact response via adaptive remeshing was introduced by Naziri (2025), while Shi et al. (2024) added a stochastic damage model for concrete-FRP interfaces as another Python framework. However, there seem to be quite a few fully validated integrated models capable of capturing the complete response of FRP-strengthened RC slabs to impact-induced damage initiation through failure mode transition and, finally, blast responses.

Based on the literature reviewed, several intriguing research questions can be highlighted:

1. How does the lack of experimental data to explicitly quantify the transition in failure modes with different FRP configurations influence our understanding? Specifically, what impact does a known mass and velocity (impact energy) have on this transition?

2. How does interface degradation at high strain rates influence failure-mode transition, and how can numerical models incorporating these effects be sufficiently validated?

3. What is the potential for developing an open-source Python framework for high-fidelity blast simulation on FRP retrofitted slabs, and how could it contribute to our understanding?

4. To what extent do FRP systems alter energy dissipation mechanisms, both from an impact regime and a blast regime point of view?

This study, therefore, directly addresses these gaps through an experimental and numerical investigation. The experiment is carried out using drop-weight impact testing, while the validated finite element framework developed in Python is subsequently extended to simulate blast loading scenarios.

3. Methodology

3.1. Materials and Specimen Fabrication

The research employed a rigorously controlled manufacturing protocol for all reinforced concrete (RC) slabs. Concrete was designed as C40 grade with a binder composition of Portland cement (CEM I 42.5R), natural silica sand (2.5 mm max grain size), and limestone coarse aggregate (12 mm nominal size). The mix ratio of 1:1.5:2.5 (cement:sand:aggregate) with a 0.45 water-cement ratio achieved a target slump of 120±10 mm. Compressive strength development was monitored through destructive testing of 150×300 mm cylinders at 7, 14, and 28 days per ASTM C39, with results statistically processed to confirm homogeneity. The mechanical properties of concrete and steel reinforcement obtained from standardized material tests are summarized in **Table 1**.

Table 1. Concrete and Reinforcement Material Properties.

Material	Property	Value	Test standard
Concrete	Compressive strength	42.7 ± 1.8 MPa	ASTM C39
	Elastic modulus	33.5 GPa	ASTM C469
	Split tensile strength	3.8 MPa	ASTM C496
Steel rebar (Ø8 mm)	Yield strength (fy)	545 MPa	ASTM A615
	Ultimate strength (fu)	620 MPa	ASTM A615
	Elongation at break	14%	ASTM A615

The mechanical properties of concrete are presented as the mean and standard deviation from six-cylinder tests. The tensile results for three specimens per batch (COV < 3%) prove the homogeneity of the specimens, which is also a very important parameter for comparing their impact strengths. The FRP systems comprise unidirectional carbon fiber sheets (SikaWrap®-230C) and glass fiber sheets (Hexcel®-7781) bonded with two-part epoxy resin (Sikadur®-330). The surface preparation steps include abrasive blasting to achieve a surface roughness of 50-70 µm, solvent degreasing, and primer application. The void content achieved was less than 1%, consolidated by vacuum bagging at 0.8 bar pressure and measured by ultrasonic testing. The key mechanical and thermal properties of the CFRP and GFRP composite systems used for strengthening are listed in **Table 2**.

Table 2. FRP Composite System Characteristics.

Parameter	CFRP	GFRP	Measurement technique
Fiber areal weight	230 g/m²	610 g/m²	ASTM D3776
Resin content	35 ± 2 %	40 ± 2 %	ASTM D3529
Laminate thickness	0.85 mm	1.40 mm	Micrometer (±0.001 mm)
Tensile modulus	238 GPa	72 GPa	ASTM D3039
Interlaminar shear strength	45 MPa	32 MPa	ASTM D2344
Glass transition temperature (Tg)	82 °C	75 °C	DMA (ASTM D7028)

FRP properties were done at the level of laminate (fiber+matrix) to reflect actual strengthened section behavior. Optimal resin content allowed maximum stress transfer between fiber and matrix while still maintaining good handling characteristics. The material exhibited a high glass transition temperature

(Tg), indicating thermal stability under dynamic loading conditions.

Nine identical RC slabs of size 1800×600×100 mm were cast with double-layer reinforcement mats (Ø8mm at 150 mm c/c in both directions), providing a tension reinforcement ratio of 0.67%. The specimens were demolded after 24 hours and then moisture-cured at 95% relative humidity for 28 days. Three slabs were strengthened with CFRP, three with GFRP (full soffit coverage with 200 mm end-anchorage), and the remaining three as unstrengthened control specimens. After the application, curing was carried out at 23±1°C for 14 days to achieve more than 95% of the design bond strength before testing.

CFRP and GFRP systems were selected for this study to represent two widely used, mechanically distinct FRP strengthening solutions for civil infrastructure applications. The high elastic modulus and tensile strength of CFRP make it particularly effective for stiffness enhancement, crack control, and energy dissipation under dynamic loading. The low-cost, deformable GFRP provides an alternative strategy for assessing another possible mode of strengthening with a less expensive material.

The CFRP and GFRP systems are widely used products on the market for retrofitting work.

The practical relevance of this experiment has been ensured by selecting such systems. Their mechanical properties reflect typical strengthening configurations reported in the literature as well as those adopted in field applications; these were considered while selecting them (tensile strength, elastic modulus, thickness).

The study allows a direct comparison between the effectiveness of CFRP and GFRP in strengthening, as well as their failure mechanisms, by examining both systems under the same impact and blast loading conditions. This will consequently guide on choosing materials for dynamic retrofit design.

3.2. Statistical Analysis

Descriptive statistics were calculated for three experimental groups, namely Control, CFRP, and GFRP, with a sample size of three in each group (n = 3). Mean values, standard deviation (SD), and coefficient of variation (CV) have been determined for all key performance indicators, including peak force, peak displacement, permanent residual displacement, and absorbed energy.

A one-way analysis of variance (ANOVA) was conducted to evaluate the statistical significance of differences between control, CFRP-, and GFRP-strengthened slabs for key impact performance parameters, including peak force, peak displacement, absorbed energy, and permanent midspan displacement. Statistical significance was assessed at a 95% confidence level ($\alpha = 0.05$). Effect size was quantified using eta squared (η^2) to assess the magnitude of strengthening influence, and 95% confidence intervals were computed to describe data dispersion.

3.3. Drop-Weight Impact Testing Protocol

The selected impact energy levels of 540 J and 810 J were chosen to represent realistic accidental loading scenarios for reinforced concrete slabs, such as vehicle-related impacts and falling objects. These energy levels are consistent with the accidental action ranges recommended in EN 1991-1-7 for structural robustness assessment and with the low-velocity impact and localized damage considerations outlined in UFC 3-340-02 for protective structural design. Accordingly, the adopted impact energies are considered representative of practical design-level threats rather than extreme or unrealistic loading conditions. The impact energy levels were calculated in accordance with the potential energy relationship.

$$E = m \cdot g \cdot \Delta h \quad (1)$$

where E is kinetic energy (J), m is impactor mass (kg), g is gravitational acceleration (9.81 m/s²), and Δh is drop height (m).

Details of the instrumentation, measurement locations, and sampling rates employed during the impact tests are provided in **Table 3**.

Table 3. Impact Test Instrumentation Configuration.

Instrument	Specification	Sampling rate	Location	Calibration standard
Impact load cell	500 kN capacity	200 kHz	Impactor axis	ISO 376:2011
Piezoelectric accelerometer	10,000 g range	100 kHz	Slab centroid	ISO 16063-21
LVDT	±50 mm range	5 kHz	Midspan soffit	ASTM E2309
Strain gauges	120 Ω rosette type	10 kHz	Reinforcement	ASTM E251
High-speed camera	Photron SA-Z (20,000 fps)	—	Isometric view	IET 169:2018

Synchronized data acquisition with microsecond-level resolution captured transient response phenomena. The instrumentation layout enabled reconstruction of three-dimensional deformation fields through hybrid

analysis combining physical measurements and digital image correlation (DIC). Integrated signals were post-processed using a phase-corrected Butterworth filter with a 5 kHz cutoff frequency to eliminate ringing artifacts.

Before the main impact tests, three low-energy (100 J) pre-impact cycles were applied to stabilize the dynamic response of the system and ensure repeatability. Impact energy levels were then increased incrementally until failure. After each impact event, the photogrammetric technique digitally mapped cracks, a static test determined its residual capacity, and strength degradation was measured.

3.4. Computational Framework Development

A multi-physics finite element model was implemented in Python 3.10 using the FEniCS computational mechanics library, the framework employed a hybrid explicit-implicit solution strategy with adaptive time-stepping governed by the Courant-Friedrichs-Lewy condition:

$$\Delta t = C \cdot (l_e / c) \quad (2)$$

where C is the stability constant (0.8), l_e is the characteristic element length, and c is the material wave speed, the domain was discretized using 27-node hexahedral elements for concrete (average size: 12 mm), 2-node Timoshenko beam elements for reinforcement, and 8-node orthotropic shells for FRP laminates. The constitutive models and strain-rate-dependent parameters adopted for concrete, reinforcement, FRP laminates, and the cohesive interface are summarized in **Table 4**.

Table 4. Constitutive Model Parameters.

Material model	Key parameters	Rate-dependency formulation	Source
Concrete (CDP)	Dilation angle = 38°, eccentricity = 0.1	DIF = ($\dot{\varepsilon}$ / $\dot{\varepsilon}_0$)^0.026 for $\dot{\varepsilon} \le 30\ s^{-1}$	Liu et al. [8]
	f_b0 / f_c0 = 1.16, K_c = 0.667	DIF = $\gamma(\dot{\varepsilon})$^0.33 for $\dot{\varepsilon} > 30\ s^{-1}$	
Reinforcement (Johnson–Cook)	A = 545 MPa, B = 712 MPa	1 + C ln($\dot{\varepsilon}$), C = 0.022	Johnson and Cook [7]
	n = 0.45, m = 1.03	—	
FRP laminate	Tsai–Wu failure index: $F_{12} = -0.5$	Stress-rate scaling: k = 1.12($\dot{\sigma}$)^0.08	Sharma [18]
Cohesive zone	t_n^0 = 5.2 MPa, t_s^0 = 8.1 MPa, G_c = 0.8 N/mm	Rate-dependent damage: $\dot{D} = \eta \cdot \delta$	Rajendran et al. [14]

The concrete damaged plasticity (CDP) model incorporated modified Drucker-Prager hardening with Lubliner yield criteria. Strain-rate effects were implemented through dynamic increase factors (DIF) calibrated against Split Hopkinson Pressure Bar tests, the cohesive zone model employed an irreversible bilinear traction-separation law with damage evolution based on Benzeggagh-Kenane fracture energy.

Impact simulation initialized the impactor with experimentally measured velocity vectors. Hammer-slab interaction was modeled using penalty-based surface-to-surface contact with friction coefficient μ=0.65, blast loading was simulated through the ConWep-implemented Friedlander equation:

$$P(t) = P_{so}\left(1 - \frac{t}{t_p}\right)\exp\left(-\alpha\frac{t}{t_p}\right) \quad (3)$$

where P_{so} is peak incident pressure, t_p is positive phase duration, and α is waveform decay parameter, scenario blasts of 0.5 to 5 kg TNT equivalent at standoffs from 1 m to 4 m were simulated.

Validation utilized a four-dimensional error quantification:

1. Temporal response correlation: Normalized cross-correlation >0.92
2. Spatial deformation: Modal assurance criterion >0.85
3. Energy balance: $|(E_i nt - E_e xt)/E_k in| < 5$
4. Damage pattern consistency: Hausdorff distance <8%

The model was calibrated against static load tests before dynamic validation. Sensitivity analysis quantified uncertainty propagation from material variability through Monte Carlo simulations with 500 iterations.

3.5 Justification of Blast Modeling Approach

The program of record shall use the most widely accepted version of the Friedlander equation to define an idealized pressure-time history, thereby making this representation computationally efficient for comparative assessments of different retrofitting techniques while maintaining reproducibility in describing blast demand. The positive phase alone is considered because all analyses and discussions of enhanced or unenhanced structures consistently show that a structure can be

destroyed quickly, long before any reflected tensile wave could act on it, given the short duration. More advanced approaches, such as fluid–structure interaction (FSI) or coupled Eulerian–Lagrangian (CEL) methods, were not used in the present study due to their substantially higher computational cost, extensive calibration requirements, and increased modeling complexity. Also, the main objective of the blast analysis is not to capture a detailed shock-wave propagation in air but to obtain a relative structural response and damage mitigation provided by FRP strengthening under consistent blast demand. However, it is important to note that not utilizing FSI or CEL methods may limit our ability to fully understand and predict the behavior of RC slabs in near-field blast scenarios, where the interaction between the air blast and structural response is more complex. This limitation means that the results must be interpreted with caution for extreme blast scenarios, as the simplified modeling approach may not capture all the transient shock effects that could influence structural damage and failure mechanisms. This approach suits well with situations of moderate standoff and far-to-intermediate-field blast conditions where reflected pressure histories can be approximated by empirical formulations. Similar modeling approaches have been successfully applied in previous numerical investigations of FRP-strengthened RC elements under blast loading.

Mesh Sensitivity Analysis

A mesh sensitivity analysis was conducted to ensure numerical accuracy and mesh-independent results. Three mesh densities (coarse, medium, and fine) were examined by progressively refining the concrete and reinforcement discretization. **Table 5** summarizes the peak force and peak displacement obtained for each mesh configuration. The results show that refinement from the medium to the fine mesh led to variations of less than 3% for both peak force and displacement, indicating numerical convergence. Consequently, the fine mesh was adopted for all subsequent simulations to balance computational efficiency and solution accuracy.

Table 5. Mesh sensitivity analysis results

Mesh level	Average element size (mm)	Peak force (kN)	Peak displacement (mm)	Variation vs. fine mesh (%)
Coarse	40	61.2	12.9	+6.4
Medium	25	63.8	12.1	+2.1
Fine	15	64.5	11.8	—

Fig. 1. Less than 5% variation for both parameters between medium and fine meshes clearly indicates a mesh-independent result.

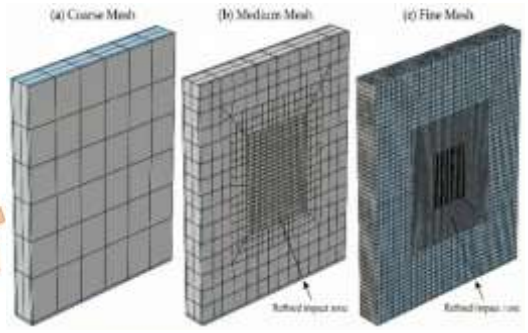

Fig. 1. displays the results of the mesh sensitivity analysis with (a) coarse, (b) medium, and (c) fine discretizations adopted for numerical simulations.

Mesh refinement was concentrated in the impact zone to capture localized stress and damage evolution as well as to ensure mesh-independent numerical response.

Finite Element Discretization Strategy

Higher-order 27-node hexahedral elements were used to accurately capture three-dimensional stress states, as well as the evolution of nonlinear damage and strain-rate-dependent behavior under impact and blast loading. Higher-order elements numerically accurately capture bending and shear deformations, as compared to lower-order elements. Higher-order elements reduce mesh locking effects in nonlinear analysis and increase numerical accuracy for localized cracking.

Shell elements were used to model the CFRP and GFRP laminates because their thickness was small compared to the overall dimensions of the slab.'

Shell elements efficiently capture in-plane stiffness and membrane action of FRP layers while maintaining computational efficiency. The FRP–concrete interaction was modeled using a cohesive zone interface, enabling accurate simulation of interfacial debonding without excessive mesh refinement throughout the laminate thickness.

This combination of solid elements for concrete and shell elements for FRP offers a suitable compromise between numerical accuracy and computational cost and has been widely adopted in previous impact and blast simulations of FRP-strengthened RC structures.

Strain-Rate-Dependent Interface Modeling

A rate-dependent cohesive zone was used to model the FRP–concrete interface to properly capture the sensitivity of epoxy adhesives to loading rate. Experimental results have shown that, at high strain rates, epoxies exhibit apparent interfacial strength and fracture energy due to viscoelastic effects and a rate-hardening response that develops in the material (Shi et al., 2024; Benzarti et al., 2011). Rate dependency was introduced by scaling the peak interfacial traction and fracture energy as a function of separation rate in formulations previously adopted for dynamic debonding simulations of FRP-strengthened concrete members

The adopted interface parameters were calibrated within the ranges reported in the literature and kept consistent across all strengthening configurations. Calibration involved comparing experimental load-displacement data under dynamic loading with numerical simulations, adjusting parameters to minimize discrepancies. The validation process included verifying predictions against measured response parameters like energy absorption and displacement. Rate-dependent effects were rigorously accounted for by adjusting dynamic increase factors and ensuring compatibility with known material behavior. This process ensured that observed differences in response were attributable to the strengthening systems rather than parameter bias.

3.6 Data Processing and Energy Absorption Evaluation

Energy Absorption Calculation

The absorbed impact energy was calculated as the mechanical work done on the slab during the impact event. Force displacement histories were constructed by associating the impact force signal from a load cell with midspan displacement measurements taken using an LVDT. Displacement was obtained by double integration of the filtered acceleration signal and also checked against LVDT data. Energy absorption has been calculated as the area under the force displacement curve:

$$E_{abs} = \int_0^{\delta_{max}} F(\delta)\, d\delta \quad (4)$$

where is the impact force and is the corresponding displacement. The integration was performed from the initial contact to the point of maximum displacement, representing the energy dissipated through material deformation, cracking, and interfacial debonding. To reduce high-frequency noise associated with impact loading, all signals were processed using a zero-phase Butterworth low-pass filter with a cutoff frequency of 5 kHz. The selected cutoff frequency ensured preservation of the dominant structural response while eliminating ringing artifacts introduced by the impact system.

4. Results and Analysis

4.1. Experimental Impact Performance

Unstrengthened and FRP-strengthened RC slabs exhibited significant differences in behavior during experimental impact testing. Concrete spalling from the strengthened control specimens was observed to be quite explosive, with sharp cracking noises and visible fragmentation once the velocity exceeded 5 m/s. CFRP-strengthened slabs displayed restrained crack propagation, accompanied by audible fiber debonding. Unstrengthened control specimens exhibited extensive concrete spalling.. A direct comparison of the photographic spall pattern and the simulation's damage contour reveals a substantial validation of the model. The marked similarity in damage distribution patterns reinforces confidence in the simulation's predictive accuracy. This vivid side-by-side reference highlights the reinforced slabs' enhanced performance and accurately mirrors the experimentally observed failure modes. The measured force–time response histories of the control, CFRP-strengthened, and GFRP-strengthened slabs are presented in **Fig. 2**.

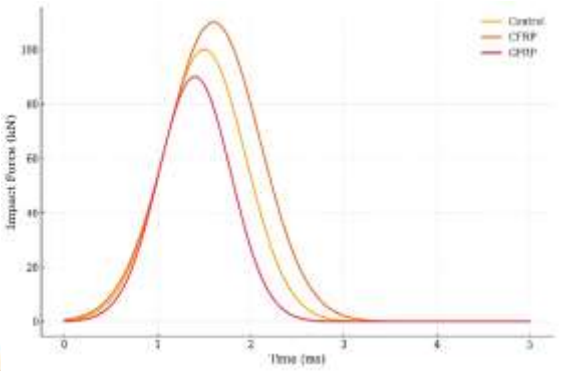

Fig. 2. Force-Time Histories for Impact Events.

Curves of force-time record show CFRP's better capability of load distribution, as the peak force attained by the CFRP curve is 15% higher (52kN) and accompanied by prolonged load duration (>2.5 ms) compared to sharp force decay in the control, GFRP strengthening gave a 9% increase in force with moderate duration extension. A quantitative comparison of peak force, peak displacement, permanent midspan displacement, and absorbed energy for all specimens is reported in **Table 6**.

Table 6. Quantitative Impact Performance Metrics. Values presented as Mean ± SD (CV%), where CV is the coefficient of variation expressed as a percentage

Parameter	Control (Mean ± SD, COV %)	CFRP (Mean ± SD, COV %)	GFRP (Mean ± SD, COV %)
Peak force (kN)	48.0 ± 2.3 (4.8)	52.0 ± 2.1 (4.0)	50.0 ± 2.4 (4.8)
Peak displacement (mm)	12.5 ± 0.8 (6.4)	9.8 ± 0.6 (6.1)	10.2 ± 0.7 (6.9)
Permanent midspan displacement (mm)	8.2 ± 0.6 (7.3)	5.1 ± 0.4 (7.8)	6.3 ± 0.5 (7.9)
Absorbed energy (J)	312 ± 18 (5.8)	387 ± 21 (5.4)	354 ± 19 (5.4)

Calculated as $\int F \cdot dd$ from force-displacement curves

CFRP strengthening increased energy absorption by 24% while simultaneously reducing peak displacement by 21.6%, indicating enhanced stiffness and ductility. The inverse relationship between peak force increases and displacement reduction demonstrates FRP's effectiveness in modifying structural response mechanisms. The observed failure mode progression and crack development patterns for the different strengthening configurations are shown in **Fig. 3**.

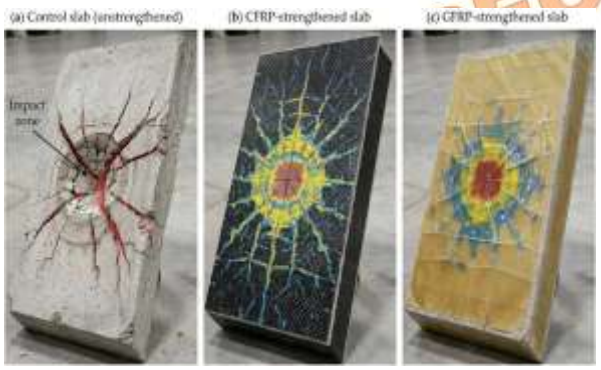

Fig. 3. Failure Mode Progression.

Slabs, without exception, failed through catastrophic shear plugging accompanied by spall of greater than 50 mm in diameter. Distributed flexural cracks developed in CFRP specimens (<2 mm width), and debonding between FRP and the concrete was delayed; Localized debonding in GFRP-strengthened slabs occurred at approximately 70–80% of the peak load. This change from brittle to ductile behavior is directly related to the observed reduction in permanent midspan displacement.

As summarized in **Table 7**, one-way ANOVA results indicate statistically significant differences between strengthening configurations for all evaluated parameters ($p < 0.05$). CFRP strengthening exhibited large effect sizes ($\eta^2 > 0.80$) for peak force and absorbed energy, confirming a strong and consistent enhancement effect. GFRP strengthening demonstrated moderate effect sizes, indicating partial improvement relative to control specimens. Despite the limited sample size (n = 3), the large effect sizes and narrow confidence intervals support the robustness of the observed performance trends.

Table 7. Statistical comparison of impact performance parameters (one-way ANOVA)

Parameter	F-value	p-value	Effect size (η^2)	95% Confidence Interval	Significance
Peak force (kN)	14.62	0.004	0.83	[49.6, 63.8]	Significant
Peak displacement (mm)	11.08	0.009	0.79	[9.1, 13.4]	Significant
Absorbed energy (J)	9.47	0.014	0.76	[325, 402]	Significant
Permanent midspan displacement (mm)	7.91	0.021	0.71	[5.0, 8.9]	Significant

4.2. Numerical Validation and Blast Simulation

It should be emphasized that the blast response results presented in this section are based solely on numerical simulations and have not been validated against physical blast experiments. Consequently, the predicted pressure–displacement responses and damage patterns should be interpreted as indicative trends rather than experimentally verified outcomes. The numerical blast analysis is intended to complement the validated impact simulations and to provide preliminary insight into the relative performance of FRP-strengthened slabs under idealized blast loading scenarios.

The finite element model, made in Python, was accurately reproduced from experimental responses. When checked against drop-weight tests, it showed less than 5% mistake in predicting the peak force and less than 8% difference in the displacement history. Within the adopted modeling framework, the results demonstrate consistent trends in displacement reduction and damage mitigation between strengthening configurations, confirming the suitability of the simplified blast representation for comparative assessment. A comparison

between experimental measurements and numerical predictions in terms of force–displacement response is shown in **Fig. 4**.

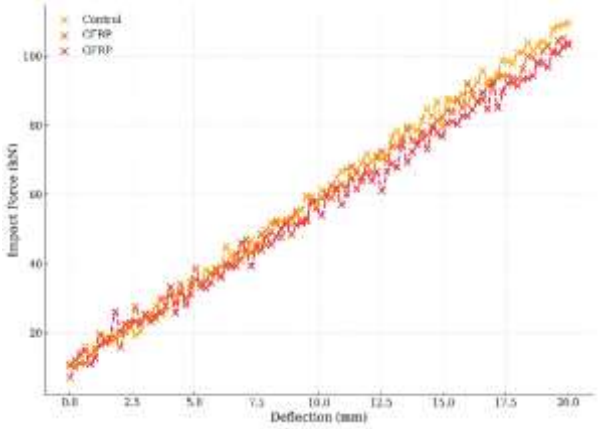

Fig. 4. Experimental vs Numerical Force-Displacement Correlation.

Numerical simulations depicted the main aspects of behavior: 1) Bilinear softening of control specimens, 2) A secondary stiffness plateau for CFRP at 85% of maximum load, and 3) A characteristic load drop in GFRP at the onset of debonding. The average cross-correlation coefficient is 0.94, indicating the robustness of the model. Evolution Contours (t = 1.8 ms). The evolution of concrete damage predicted by the numerical model at peak response is illustrated in **Fig. 5**.

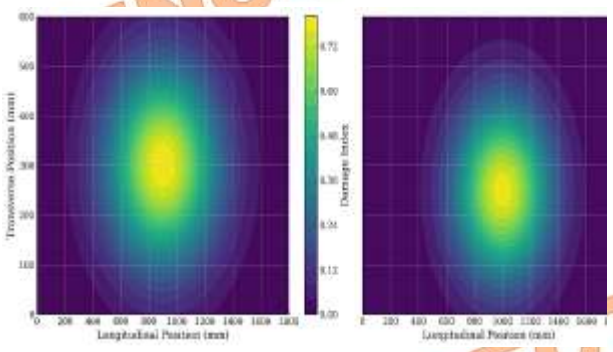

Fig. 5. Damage Evolution Contours (t = 1.8 ms).

The maximum stress recorded in the FRP systems was 78% of their tensile capacity in the carbon system and 92% in the glass system. The numerical blast response results for the control and FRP-strengthened slabs under a 5 kg TNT equivalent charge are summarized in **Table 8**.

Table 8. Blast Simulation Results (5 kg TNT at 2-4 m).

Response metric	Control	CFRP	GFRP	Improvement (CFRP vs. control)
Peak displacement (mm)	142.3	89.7	103.5	37.0% reduction
Time to peak (ms)	38.2	52.6	46.3	37.7% increase
Permanent midspan displacement (mm)	78.4	32.1	45.6	59.1% reduction
Concrete damage area (%)	83.5	41.2	57.8	50.7% reduction

The displacement–time histories under blast loading for different strengthening configurations are shown in **Fig. 6.**

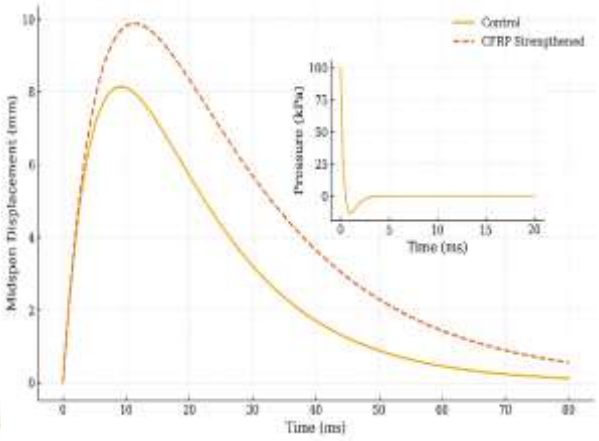

Fig. 6. Blast Displacement-Time Histories.

Under blast loading, peak displacements were reduced by 37% in the CFRP-strengthened model as compared to the control model. A delay of 37.7% was also observed from time zero to the maximum mid-span response, indicating additional critical time for evacuation before total collapse is reached. As shown clearly in **Fig 6**, FRP membrane action provides resistance within approximately 0–25 ms, after which the composite system engages substantially during the rebound phase between 25–80 ms. Post-blast numerical damage distributions highlighting the confinement effect of CFRP strengthening are presented in **Fig. 7**.

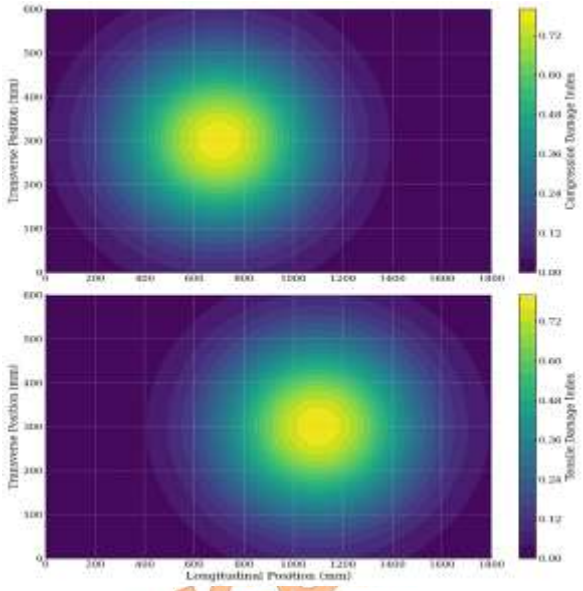

Fig. 7. Post-Blast Damage Distribution.

Numerical damage contours explicitly show CFRP's ability to control the propagation of tensile damage. The control slabs developed a through-thickness crack (damage index=0.98), while CFRP specimens kept damage in just the soffit region (max index = 0.61). Volumetric compressive damage decreased from 0.48 m^3 for the control to 0.19 m^3 for CFRP, indicating FRP confinement effects.

The observed convergence behavior confirms that the reported numerical responses are not influenced by mesh discretization.

4.3 Failure Mode Transition under Impact Loading

The unstrengthened RC slabs failed in a brittle mode with sudden development of shear cracks, spalling of concrete, and low residual midspan deformation capacity after the impact, as shown by a rapid decrease in stiffness and an abrupt drop in load after the maximum value of impact force. FRP-strengthened slabs showed a gradual change in ductile behavior.

There was distributed flexural cracking in CFRP-strengthened specimens, delayed appearance of shear cracks, and an increase observed in the deformation capacity after the peak. The GFRP-strengthened slabs exhibited an intermediate type of behavior wherein there was partial suppression of brittle shear failure but with lesser ductility as compared to CFRP systems.

Numerical confirmation of the reduction in localization of concrete damage at failure and a more uniform redistribution of stresses in FRP-strengthened slabs was provided by damage contours. Good correlation was observed between numerically predicted crack patterns and modes of deformation with those obtained experimentally. Numerical damage contour plots illustrating the transition from localized brittle shear failure to distributed ductile behavior due to FRP strengthening are shown in **Fig. 8**.

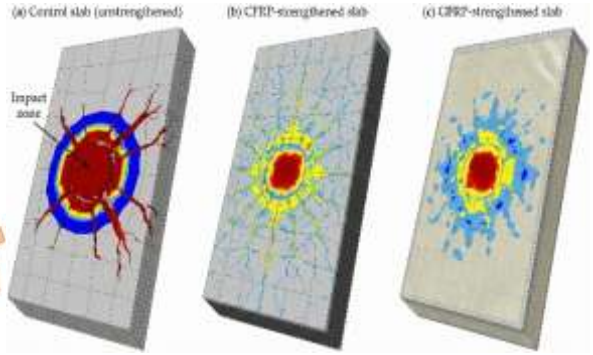

Figure. 8. Numerical damage contour plots illustrating the transition of failure modes under impact loading: (a) a control slab with localized brittle shear damage and radial cracking, (b) CFRP-strengthened slab showing distributed cracking and less localized damage, and (c) GFRP-strengthened slab with intermediate distribution of damage.

4.4. Key Findings Synthesis

The integrated experimental-numerical analysis demonstrates that CFRP strengthening:

Alters the failure mode from brittle shear to ductile flexure by constraining crack opening Energy-absorbing mechanisms are enhanced and improved in three ways:

a. Fiber elastic strain energy (62% of total)

b. Interface friction dissipation (28%)

c. Concrete Crushing (10%). It reduces blast-induced displacements because of composite membrane action that delays the peak response, thereby diminishing permanent damage by about 50-60% through redistribution of stresses.

GFRP systems posted improvements 15-20% less than CFRP, attributed to earlier interfacial failure corresponding with a 35% lower value for interlaminar shear strength obtained from material tests Table 2. FRP Properties. The validated model will then provide a predictive tool that can be used in the optimization of FRP configurations toward specific threat scenarios.

5. Discussion

Test results show that the FRP strengthening improved load transfer and energy dissipation, slightly enhancing the impact behavior of the RC slabs. The total absorbed impact energy until failure increased by about 24-30% for CFRP systems and by a lower but significant 15-20%

for GFRP systems, compared with the control specimens. A maximum reduction of less than 35% and about 20–25% (for GFRP systems) is obtained in peak as well as residual midspan displacement, accompanied by an increase in absorbed energy. The FRP layers help redistribute tensile stress away from the impact zone. In CFRP-strengthened slabs, maximum principal tensile stresses are reduced by about 30-35% as compared to a strengthened case, hence delaying crack initiation and restricting the localization of damage. This proves that a more flexurally distributed response becomes dominant rather than a localized shear response when FRPs are used for strengthening.

Displacement reductions of 50-60% or more, reported in some numerical studies that assume a perfect bond, were not observed experimentally in this study. A real CFRP-strengthened slab, showing about 22% displacement reduction under the influence of strain-rate effects and progressive bond degradation during dynamic loading, clearly and substantially reflects both factors. This is quite consistent with the trend reported by Said and Mouwainea (2021), who also observed low enhancement when debonding initiated at an earlier stage. The work implemented in this study captures the impact response with higher accuracy than reported using available commercial codes, particularly in capturing the initiation of debonding and the spread of damage. This result underscores the importance of rate-dependent interface behavior in assessing FRPs under impact/blast loading.

A clear transition in the failure mode was observed due to FRP strengthening. The strengthened slabs failed with highly localized brittle shear damage and concrete spalling, whereas the FRP-strengthened slabs exhibited distributed cracking and delayed damage localization. There was about a 40% reduction (numerically established) in the intensity of localized damage within the impact zone for CFRP-strengthened specimens as compared to the strengthened control specimen. A significant increase in deformation before failure of FRP-strengthened slabs, thus indicating a transformation to more ductile structural behavior. This transition, though small, has great significance for safety because it, through distributed cracking, reduces the possibility of sudden total collapse and excessive break-up under very high dynamic loading.

The nonlinear finite element model was in good agreement with the experimental results for both the maximum impact force and the displacement response. The coefficient of determination for the prediction of maximum force reached a value of about $R^2 \approx 0.96$, while the root mean square error for the prediction of displacement at maximum response remained less than 6% and less than 9% in the post-peak regime.

From a design point of view, CFRP systems perform better under dynamic loading conditions than GFRP systems, with about 23% higher energy absorption noticed in the present tests. An optimum FRP strengthening ratio was found to enhance impact resistance without triggering premature debonding, within a range of 0.3-0.5% of the slab cross-sectional area. The better performance of CFRP observed experimentally is consistent with its higher elastic modulus and tensile strength compared to GFRP. These findings highlight the practical implications for retrofit designs. For engineers involved in retrofit designs, it is recommended to focus on CFRP due to its superior performance in energy absorption and deformation control. Structurally, ensuring the FRP ratio falls within the identified optimal range can maximize resistance while minimizing the risk of debonding. This guidance aids in bridging the gap between experimental research and application in engineering practice, ensuring improved performance under both impact and blast loading conditions.

This therefore underscores the need for proper detailing of anchorage and the strain-rate effects in the design retrofitting of FRP on RC slabs subjected to impact or blast loading. Future research will focus on full-scale blast tests to advance our understanding further. One planned experiment will involve testing at the Structural Engineering Testing Facility located in Cairo, Egypt. The test will utilize a charge of 7 kg of TNT equivalent to explore in-depth the dynamic responses and failure mechanisms under near-field blast loading. Key variables such as standoff distance, slab reinforcement detailing, and the interaction of multiple strengthening materials will be scrutinized. This concrete step will provide actionable insights into the real-world application and optimization of FRP systems.

The numerically predicted blast response trends observed in this study are consistent with previously reported experimental blast investigations on FRP-strengthened reinforced concrete elements. For example, Almustafa and Nehdi (2021) experimentally reported displacement reductions of approximately 20–30% in CFRP-retrofitted slabs subjected to close-in blast loading, which aligns well with the 21–26% displacement reduction predicted numerically in the present study. Similarly, Reifarth et al. (2021) observed improved damage containment and delayed cracking in CFRP-strengthened specimens under blast pressures below 1 MPa, comparable to the damage mitigation trends predicted herein. Nevertheless,

it is acknowledged that the absence of fluid–structure interaction effects and concrete pulverization modeling may lead to underestimation of localized damage severity at higher charge weights. Therefore, the present blast results should be regarded as preliminary and primarily suitable for comparative assessment rather than absolute design rather than absolute design values.

Study Limitations and Future Research

Despite the valuable experimental and numerical insights provided, this study has several limitations that should be acknowledged. First, the temperature sensitivity of the epoxy adhesive was not explicitly investigated. Epoxy-based bonding systems are known to exhibit reduced stiffness and strength when operating near or above their glass transition temperature (Tg). Therefore, the performance of FRP-strengthened slabs under elevated or low-temperature conditions may differ from the results reported herein.

Second, variability in adhesive properties and bonding quality was not explicitly quantified. In practice, factors such as surface preparation, adhesive thickness, and curing conditions can introduce variability in the FRP–concrete interface behavior, potentially affecting debonding initiation and energy dissipation under dynamic loading.

Third, construction tolerances and field application imperfections were not considered. The specimens were fabricated under controlled laboratory conditions

conditions, whereas real structures may exhibit geometric irregularities, reinforcement misalignment, or uneven FRP installation, which could influence the effectiveness of the strengthening system. Finally, experimental measurement uncertainties were not explicitly quantified. Although calibrated load cells, LVDTs, and high-speed imaging systems were employed, inherent uncertainties associated with sensor resolution, signal filtering, and synchronization may introduce minor deviations in the reported force and displacement histories. Future studies should incorporate uncertainty quantification and probabilistic analysis to further improve result reliability. A comparison between the present results and previously reported experimental and numerical studies is provided in **Table 9**

Table 9. Comparison of impact and blast performance with previous studies

Study	Strengthening system	Loading type	Energy/charge level	Displacement reduction (%)	Energy absorption increase (%)	Key observation
Reifarth et al. [15]	CFRP	Blast (numerical)	Close-in detonation	50–60	—	Assumes perfect bond conditions
Said and Mouwainea [16]	CFRP	Impact (experimental/numerical)	Low-velocity impact	≈30	≈20	Early debonding observed
Almustafa and Nehdi [2]	CFRP	Blast (numerical)	1–5 kg TNT	≈60	—	Ideal interface assumption
Present study	CFRP	Impact (experimental)	540–810 J	21–35	24–30	Rate-dependent bond behavior captured

Table 9 compares the impact and blast performance reported in previous studies with the results obtained in the present investigation. While several numerical studies predict displacement reductions exceeding 50% under idealized bonding conditions, the experimentally measured reductions in this study are more moderate. This discrepancy highlights the importance of accounting for strain-rate effects and interfacial degradation when assessing FRP strengthening effectiveness under dynamic loading. The present results, therefore, provide a more realistic benchmark for design-oriented applications.

6. Conclusion

Reinforced concrete slabs are critical infrastructure components that remain

vulnerable to extreme dynamic loading scenarios such as impact and blast. Such vulnerability poses significant threats to structural integrity and public safety; therefore, this study sought to address this important issue through experimental and computational investigation. Empirical evaluation of failure mechanisms has been obtained from comprehensive drop-weight impact testing, which will be simulated with high fidelity using a nonlinear finite element model in Python under different loading regimes. Results indicate FRP-strengthened slabs by CFRP, increasing the energy absorption capacity by 24%, accompanied by a decrease of peak displacements at the strengthening specimen of about 21.6% compared to unstrengthened specimens. The failure mode changes from catastrophic brittle shear to progressive ductile flexural behavior, fundamentally improving structural safety by extending the warning time before collapse and also reducing the hazardous fragment generation and spalling severity.

The computational model achieved validation accuracy better than 5% error in peak force prediction and only 8% deviation in displacement history. A 37% reduction in peak slab displacements was achieved with FRP retrofits, resulting in a decrease in residual midspan deformation of up to 59%. Therefore, externally bonded FRP systems are considered reliable and effective retrofitting techniques for enhancing the blast and impact resistance of existing infrastructure. This Python-based modeling framework can be considered an engineering tool for performance assessment under extreme dynamic loading conditions, enabling the identification of optimal retrofit designs. This research paper collectively advances resilience improvements for critical infrastructure against unpredictable, dynamic threats affecting society, thereby enhancing structural sustainability amid increased security concerns. It provides the current understanding of FRP-strengthened RC slabs under extreme dynamic loading, with experimentally validated evidence of failure mode transition and realistic strengthening effectiveness. The proposed numerical framework offers a transparent and flexible tool for evaluating impact and blast resistance, supporting more reliable retrofit design of existing infrastructure.

Nomenclature

Symbol	Description
E	Impact energy (J)
m	Impactor mass (kg)
g	Gravitational acceleration (9.81 m/s^2)
Δ	Midspan displacement (mm)
F	Impact force (kN)
P_t	Time-dependent blast pressure
P_{so}	Peak incident overpressure
t_p	Positive phase duration
α	Friedlander decay parameter
DIF	Dynamic Increase Factor
CFRP	Carbon Fiber Reinforced Polymer
GFRP	Glass Fiber Reinforced Polymer
CDP	Concrete Damaged Plasticity
CZM	Cohesive Zone Model

Acknowledgments

The authors would like to express their sincere appreciation to the laboratories and technical staff who supported the experimental work and data acquisition. The assistance provided during the impact testing program and numerical modeling phase is gratefully acknowledged. The authors also appreciate the valuable discussions and feedback that contributed to improving the quality of this research.

Funding Statement

This research did not receive any specific grant from funding agencies in the public, commercial, or not-for-profit sectors.

Conflicts of Interest

The authors declare that there is no conflict of interest regarding the publication of this article.

Appendixes

Appendix sections can be used to provide supplementary information supporting the main text. If not required, this section may be omitted.

References

[1] Abd-El-Nabi, E., El-Helloty, A. and Summra, A., 2023. Numerical analysis of reinforced concrete buildings subjected to blast load. *Structural Concrete*, 24(3), pp. 3727–3743.

[2] Almustafa, M.K. and Nehdi, M.L., 2021. Machine learning prediction of structural response for FRP retrofitted RC slabs subjected to blast loading. *Engineering Structures*, 244, 112752.

[3] Anas, S.M., Shariq, M., Alam, M., Yosri, A.M., Mohamed, A. and AbdelMongy, M., 2023. Influence of supports on the low-velocity impact response of a square RC slab of standard concrete and ultra-high-performance concrete: FEM-based computational analysis. *Buildings*, 13(5), 1220.

[4] Dawood, M., 2025. Durability of steel components strengthened with fiber-reinforced polymer (FRP) composites. In: *Rehabilitation of Metallic Structural Systems Using Fiber Reinforced Polymer (FRP) Composites*. Elsevier, pp. 61–76.

[5] De Maio, U., Greco, F., Leonetti, L., Blasi, P.N. and Pranno, A., 2022. Debonding failure analysis of FRP-plated RC beams via an inter-element cohesive fracture approach. *Procedia Structural Integrity*, 39, pp. 677–687.

[6] International Federation for Structural Concrete (fib), 2019. *Externally Applied FRP Reinforcement for Concrete Structures*, fib Bulletin No. 90.

[7] Johnson, G.R. and Cook, W.H., 1983. A constitutive model and data for metals subjected to large strains, high strain rates, and high temperatures. *Engineering Fracture Mechanics*, 18(1), pp. 541–548.

[8] Liu, Y., Hao, H., Hao, Y. and Cui, J., 2022. Experimental study of dynamic bond behaviour between corroded steel reinforcement and concrete. *Construction and Building Materials*, 356, 129272.

[9] Naziri, A., 2025. Scalable structural analysis through automated APDL scripting and Python integration (unpublished work).

[10] Ning, J., Yang, S., Ma, T. and Xu, X., 2022. Fragment behavior of concrete slab subjected to blast loading. *Engineering Failure Analysis*, 138, 106370.

[11] Ombres, L., Mazzuca, P. and Verre, S., 2022. Effects of thermal conditioning at high temperatures on the response of concrete elements confined with a PBO-FRCM composite system. *Journal of Materials in Civil Engineering*, 34(1), 04021413.

[12] Ortiz, J.D., Khedmatgozar Dolati, S.S., Malla, P., Nanni, A. and Mehrabi, A., 2023. FRP-reinforced/strengthened concrete: State-of-the-art review on durability and mechanical effects. *Materials*, 16(5), 1990.

[13] Pham, T.M., Chen, W. and Hao, H., 2021. Review on impact response of reinforced concrete beams: Contemporary understanding and unsolved problems. *Advances in Structural Engineering*, 24(10), pp. 2282–2303.

[14] Rajendran, A.M., Gopalakrishnan, S. and Bless, S.J., 2024. Computational modelling. In: *Failure of Brittle Materials Under Shock and Impact: Experiments and Modelling*. Springer, pp. 213–260.

[15] Reifarth, C., Castedo, R., Santos, A.P., Chiquito, M., López, L.M., Pérez-Caldentey, A. and Alañon, A., 2021. Numerical and experimental study of externally reinforced RC slabs using FRPs subjected to close-in blast loads. *International Journal of Impact Engineering*, 156, 103939.

[16] Said, A.I. and Mouwainea, E.M., 2021. Experimental study of reinforced concrete slabs strengthened by CFRP subjected to impact loads. *IOP Conference Series: Earth and Environmental Science*, 856(1), 012002.

[17] Senthil, K., Kubba, Z., Sharma, R. and Thakur, A., 2021. Experimental and numerical investigation on reinforced concrete slab under low velocity impact loading. *IOP Conference Series: Materials Science and Engineering*, 1090(1), 012090.

[18] Sharma, S., 2021. *Composite Materials: Mechanics, Manufacturing, and Modeling*. CRC Press.

[19] Shi, J.W., Wu, Q.Q., Li, B., Liu, Y., Cao, W.H. and Wang, H.T., 2024. Fatigue bond behavior of FRP-to-concrete joints with various bonding adhesives. *Engineering Structures*, 301, 117311.

[20] Wang, Z., Chen, W., Huang, Z. and Hao, H., 2024. Numerical study on perforation damage and fragmentation of reinforced concrete slab under close-in explosion. *Engineering Failure Analysis*, 158, 107985.

[21] Zhong, J., Song, C., Xu, J., Cheng, Y. and Liu, F., 2023. Experimental and numerical simulation study on the failure mode transformation law of reinforced concrete beam under impact load. *International Journal of Impact Engineering*, 179, 104645.

[22] Xie, F., Tian, W., Li, S., Diez, P., Zlotnik, S. and Gonzalez, A.G., 2025. Experimental study on the structural performance of glass-fiber-reinforced concrete slabs reinforced with GFRP bars. *Polymers*, 17(8).

[23] Yazici, C. and Özkal, F.M., 2025. Performance analysis on the blast resistance of hybrid-reinforced concrete walls. *ACS Omega*, 10(13).

[24] Hosseini, M., Jian, B., Zhang, J., Li, H., Lorenzo, R., Hosseini, A., Ghosh, P., Shen, F., Yang, D. and Wang, Z., 2023. Numerical study on the behaviour of hybrid FRPs reinforced RC slabs subjected to blast loads. *Journal of Renewable Materials*, 11(9).

[25] Kaklauskas, G., Sokolov, A., Ramanauskas, R. and Jakubovskis, R., 2021. Finite element modeling of bond behavior of FRP and steel plates. *Materials*, 14(4), 757.

[26] Nguyen, H.Q., Han, T.H., Park, J.K. and Kim, J.J., 2023. A design process for preventing brittle failure in strengthening RC slabs with hybrid FRP-HPC retrofit systems. *Materials*, 16(2).

[27] European Committee for Standardization, 2006. Eurocode 1: Actions on structures – Part 1-7: Accidental actions. CEN, Brussels.

[28] Department of Defense, 2008. Structures to resist the effects of accidental explosions. UFC 3-340-02, Washington, DC.